electronic reprint

STRUCTURAL SCIENCE
CRYSTAL ENGINEERING
MATERIALS

ISSN: 2052-5206
journals.iucr.org/b

Polymorphic forms of bendamustine hydrochloride: crystal structure, thermal properties and stability at ambient conditions

Pablo Gaztañaga, Ricardo Baggio and Daniel Roberto Vega

Acta Cryst. (2019). B**75**, 933–941

Acta Cryst B
STRUCTURAL SCIENCE
CRYSTAL ENGINEERING
MATERIALS
ISSN 2052-5206

Polymorphic forms of bendamustine hydrochloride: crystal structure, thermal properties and stability at ambient conditions

Pablo Gaztañaga,[a,b,c]* Ricardo Baggio[a] and Daniel Roberto Vega[a,b]

[a]Gerencia de Investigación y Aplicaciones, Centro Atómico Constituyentes, Comisión Nacional de Energía Atómica, Av. Gral Paz 1499, B1650KNA, San Martin, Buenos Aires, Argentina, [b]Escuela de Ciencia y Tecnología, Universidad Nacional General San Martín, Martín de Irigoyen, 3100, CP 1650, San Martín, Buenos Aires Argentina, and [c]CONICET (Consejo Nacional de Investigaciones Científicas y Tecnológicas), Argentina. *Correspondence e-mail: pablogzt@gmail.com

Received 4 June 2019
Accepted 2 August 2019

Edited by A. J. Blake, University of Nottingham, England

Keywords: bendamustine hydrochloride; polymorphism; crystal structure; single-crystal X-ray diffraction.

CCDC references: 1945029; 1945030; 1945031

Supporting information: this article has supporting information at journals.iucr.org/b

Crystallographic, thermal and stability analyses are presented of three different anhydrated forms of bendamustine hydrochloride [(I), (III) and (IV)] and a fourth, monohydrated one (II). Since form (I) presents the higher melting point and the higher heat of fusion, according to the 'heat of fusion' rule it should be the most stable in thermodynamic terms [Burger & Ramberger (1979). *Mikrochim. Acta*, **72**, 259–271], though it is unstable in high-humidity conditions. The monohydrate structure (II), in turn, dehydrates by heating and topotactically transform into anhydrate (III). This latter form appears as less stable than anhydrate (I), to which it is linked *via* a monotropic relationship. For these three different forms, the crystal structure has been determined by single crystal X-ray diffraction. The crystal structures and molecular conformations of forms (II) and (III) are quite similar, as expected from the topotactic transformation linking them; furthermore, under high-humidity conditions, form (III) shows changes compatible with a transformation into form (II) within 24 h. The crystal structure of form (I) is different from the other two. The remaining polymorphic form (IV) could only be obtained as a powder, from which its crystalline structure could not be determined. The relative thermodynamic stability of the different crystalline forms was determined by differential scanning calorimetry and thermogravimetrical studies, and their stability under different humidity conditions analysed.

1. Introduction

Bendamustine is a chemotherapy medication used in the treatment of chronic lymphocytic leukaemia, non-Hodgkin's lymphoma and multiple myeloma (Cheson & Rummel, 2009). The drug is a bifunctional alkylating agent consisting of a purine and amino acid antagonist (a benzimidazole ring) and an alkylating nitrogen mustard moiety. The alkylating toxicity of bendamustine is based on the disruption of the matrix function of DNA in DNA synthesis (Bremer & Roth, 1996)

Even if bendamustine action compares quite satisfactorily with the remaining alkylating agents in use, it is a hazardous drug and should be administrated with extreme care. As an additional inconvenience, shared with many other nitrogen mustards, the molecule presents a tendency to hydrolyze in water, a fact which constitutes perhaps the most significant drawback in the manufacture and delivery of the drug. Hydrolysis of the nitrogen mustard may lead to technical difficulties in its preparation and administration. Due to this instability in aqueous solution, bendamustine is currently

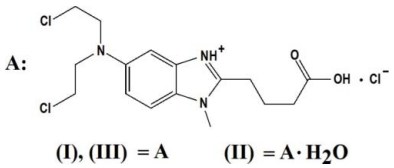

(I), (III) = A (II) = A·H_2O

provided as the bendamustine hydrochloride salt, which is supplied as a lyophilized powder for injection. Once reconstituted the drug should be administrated as soon as possible in order to avoid degradation due to hydrolysis. Lyophilized preparations of bendamustine hydrochloride can contain different amount of degradation products (Drager *et al.*, 2012; Ravikanth *et al.*, 2013) for what it is important to improve the stability of bendamustine hydrochloride and its formulations. This instability against water poses also some limitations on the type of excipients used in the formulation of the drug. For instance, mannitol, frequently used in this regard for the lyophillization process (Ravikanth *et al.*, 2013) and conventionally used in parenteral formulations (Akers, 2002), has been shown to occasionally transform into an hydrated form. The formation of a crystalline hydrate by an excipient during freeze-drying may have several inconvenient consequences, among them the unwitting formation of highly hygroscopic materials that may undergo structural relaxation during storage. The residual water that is not removed by freeze-drying may be a potential threat to product stability if it is released during storage (Yu *et al.*, 1999).

Summarizing: the complex behaviour which bendamustine may present in its interaction with water (in particular with ambient humidity) shows the need of

(*a*) a detailed characterization of the drug in its various crystalline states, and

(*b*) an adequate understanding of the way these forms behave, when subject to different dampness/dryness conditions. Both items constitute the scope of the work we have undertaken in the present report.

The forms of bendamustine hydrochloride known so far (and which we shall analyze in what follows) have originally been reported in a US Patent Application (Cooper *et al.*, 2009). In this patent Cooper and coworkers describe (in the succinct language typical of patents) three different crystalline forms of anhydrated bendamustine hydrochloride [named therein (I), (III) and (IV)] and one monohydrated form (II). A single-crystal X-ray diffraction (SCXRD) study of the most stable form (I) is reported, but no structural information is given on the remaining ones. Form (III), in turn, is described as obtained by dehydration of form (II). All four forms are identified by their X-ray powder diffraction (XRPD) diagrams, and some further thermal information is also provided (melting points, *etc*). On the other hand, the only bendamustine hydrochloride crystal structure appearing in the Cambridge Structural Database (CSD) (Groom *et al.*, 2016) is the hydrated form (II), reported as a private communication (Reck, 2006: entry NEQGUM) though refined to a very low resolution (1.10 Å). No information could be found in the literature regarding the crystal structure of forms (III) and (IV).

In the present work we report a structural SCXRD analysis of forms (I), (II) and (III) [we use the same labelling used by Cooper *et al.* (2009) for the different forms]; we analyze by thermogravimetry (TGA) the hydration states and thermal stability of the different crystalline forms and determine the relative thermodynamic stability of the different crystalline forms, as assessed by differential scanning calorimetry (DSC) experiments.

Finally, the behaviour of forms (I), (II) and (III) is analyzed under different humidity conditions, as a way to determine eventual problems which may appear in the formulation, when using different crystalline forms as the starting API.

2. Experimental

2.1. Crystallization

The starting material for all the crystallization essays was the monohydrated form (II), kindly provided by Eriochem, and its provision is gratefully acknowledged. Excellent single crystals of form (I) used in SCXRD were obtained by slow evaporation from an isopropanol solution of bendamustine hydrochloride monohydrate in a dry environment at ambient temperature. Those for the monohydrated form (II) were not of high quality. The best ones were grown from recrystallization of an acetone solution of the monohydrated form at −15°C. Finally, poor single crystals of form (III) were obtained from the *in situ* topotactic dehydration of single crystals of form (II), (a process performed in a 800 Series Cryostream Cooler unit, from Oxford Cryosystems) by slowly heating the samples (1°C min^{-1}) from room temperature up to 77°C .

Although no single crystals could be grown for form (IV), a crystalline powder was obtained by thermal treatment at 50°C for one day of amorphous bendamustine hydrochloride. The amorphous form, in turn, was obtained by supercooling molten bendamustine hydrochloride [m.p. (II): 155°C] at ambient temperature. The process was performed in a 101-OAB Electric Heated Blast Dry Box, from Tianjin City Taisite Instrument Co. Ltd.

2.2. Stability under different humidity conditions

In order to study the stability of the different crystalline species under different humidity conditions, forms (I), (II) and (III) were put in a desiccator with a liquid water reservoir. Mass gain was measured in a Mettler AJ150 microbalance; the samples were monitored through their XRPD patterns, obtained at regular intervals. On the other hand, the stability of form (II) under dryness conditions was studied in a similar way, by replacing the liquid water reservoir by silica gel. All these experiments were performed at ambient temperature.

2.3. Instrumental techniques

TGA studies were performed with a Shimadzu DTG-50 apparatus, while a TA instrument, model Q2000 was used for DSC. In both cases, the experiments were carried out under a N_2 atmosphere, with a 10 ml min^{-1} flux. SCXRD data of (I) and (III) were collected at T = 150 K while those for (II) was collected at T = 100 K on a Bruker D8 Quest Eco diffractometer using Mo $K\alpha$ radiation (λ = 0.71073 Å) with a 800 Series Cryostream Cooler manufactured by Oxford Cryosystems. XRPD data were obtained using a Panalytical

Table 1
Experimental details.

Experimental were carried with Mo $K\alpha$ radiation using a CCD Oxford Diffraction Xcalibur, Eos, Gemini. Absorption correction using multi-scan *CrysAlis PRO* (Oxford Diffraction, 2009). H atoms were treated by a mixture of independent and constrained refinement.

	(I)	(II)	(III)
Crystal data			
Chemical formula	$C_{16}H_{22}Cl_2N_3O_2{\cdot}Cl$	$C_{16}H_{22}Cl_2N_3O_2{\cdot}Cl{\cdot}H_2O$	$C_{16}H_{22}Cl_2N_3O_2{\cdot}Cl$
M_r	394.71	412.73	394.71
Crystal system, space group	Monoclinic, *C*2/*c*	Monoclinic, $P2_1/c$	Monoclinic, $P2_1/c$
Temperature (K)	150	100	150
a, *b*, *c* (Å)	23.0502 (6), 6.7836 (2), 25.4596 (7)	4.6490 (6), 47.213 (5), 8.9051 (10)	4.722 (4), 45.671 (19), 8.798 (7)
β (°)	114.262 (1)	96.222 (7)	97.66 (6)
V (Å^3)	3629.33 (18)	1943.1 (4)	1880 (2)
Z	8	4	4
μ (mm^{-1})	0.52	0.49	0.50
Crystal size (mm)	0.42 × 0.38 × 0.12	0.24 × 0.06 × 0.04	0.48 × 0.18 × 0.14
Packing index†	70.2	69.3	67.7
Data collection			
T_{min}, T_{max}	0.84, 0.96	0.92, 0.96	0.84, 0.94
No. of measured, independent and observed [$I > 2\sigma(I)$] reflections	64 102, 8857, 6634	19 169, 3545, 2180	34 373, 3384, 2612
R_{int}	0.056	0.188	0.131
(sin $\theta/\lambda)_{max}$ (Å^{-1})	0.836	0.600	0.600
Refinement			
$R[F^2 > 2\sigma(F^2)]$, $wR(F^2)$, S	0.044, 0.112, 1.03	0.081, 0.157, 1.10	0.171, 0.379, 1.24
No. of reflections	8857	3545	3384
No. of parameters	224	239	225
No. of restraints	2	5	23
	$w = 1/[\sigma^2(F_o^2) + (0.0488P)^2 + 3.3772P]$ where $P = (F_o^2 + 2F_c^2)/3$	$w = 1/[\sigma^2(F_o^2) + (0.0253P)^2 + 8.2062P]$ where $P = (F_o^2 + 2F_c^2)/3$	$w = 1/[\sigma^2(F_o^2) + 62.7847P]$ where $P = (F_o^2 + 2F_c^2)/3$
$\Delta\rho_{max}$, $\Delta\rho_{min}$ (e Å^{-3})	0.79, −0.78	0.40, −0.51	0.71, −0.81

Computer programs: *CrysAlis PRO* (Oxford Diffraction, 2009), *SHELXS* (Version 2013/1; Sheldrick, 2008, *SHELXL2018/1* (Sheldrick, 2018), *XP* in *SHELXTL* (Sheldrick, 2008). † Defined in Kitaigorodskii (1961) and calculated using *PLATON* (Spek, 2009).

Empyrean diffractometer with Cu $K\alpha$ radiation (λ = 1.54178 Å).

2.4. Refinement of the SCXRD models

The initial models were obtained by direct methods (*SHELXS*; Sheldrick, 2008), completed by successive Fourier synthesis and refined by least-squares on F^2 (*SHELXL*; Sheldrick, 2015). The final R factors were in direct relationship to the quality of the available crystals, as described in 2.1, for instance (I) (excellent specimens), R = 0.0436, (II) (medium quality crystals), R = 0.0814; (III) (poor samples obtained from a topotactic dehydration), R = 0.1714 (see Table 1).

All H atoms were originally found in difference maps, but treated differently in refinement. The O—H and N—H ones were refined with restrained O—H = N—H = 0.85 (2) Å, U(H) = 1.2 × U_{equiv}(host) while (C—)H atoms were repositioned in their expected positions and allowed to ride with U(H) = x × U_{equiv}(C) [d(C—H_{arom}) = 0.95 Å, x = 1.2; d(C—$H_{methylene}$) = 0.99 Å, x = 1.2; d(C—H_{methyl}) = 0.98 Å, x = 1.5]. One of the water hydrogens in (II) (H1*WA*) makes a very strong hydrogen-bond to Cl1 (entry #10 in Table 2) with a sensible enlargement of the O—H distance in spite of the restraints applied. The remaining hydrogen atom (H1*WB*), instead, with a weaker interaction to Cl1 behaves in a normal way (entry #11 in Table 2).

Due to the low quality of the dataset collected for (III), RIGU restraints were needed in order to achieve stable refinement.

3. Results and discussion

3.1. Crystal and molecular structure

Table 1 presents some crystal and refinement parameters for forms (I), (II) and (III), while Fig. 1 shows ellipsoid plots of their molecular structures. All three present a similar planar nucleus, (the one going from C4 to N3; mean/max RMS deviations from plane (in Å). (I): 0.0033, 0.0076 (for C5); (II): 0.0119, 0.0329 (for N3); (III): 0.0176, 0.0483 (for N3). This planarity can be assessed in Fig. 2 where a least-squares fitting of this nucleus in the three molecules is shown. The similarity of the planar groups as well as the departures of the side chains at both sides are apparent from inspection. The most obvious are the C4—C5 rotation in the butyric chain [which clearly differentiates (I) from (II)/(III)] and the C1—C2 rotation of the carboxylate group (where all three moieties differ). A similar effect can be envisaged in the nitrogen mustard side, in all three bonds involving N3 (N3—C10, N3—C11, N3—C13) mainly setting apart (I) from (II) and (III). The reasons for these differences are attributable to hydrogen bonding and will be discussed below. Quantitative details of the conformational differences can be obtained from Table 2,

which shows a selected group of torsion angles presenting the most significant differences.

The most interesting structural aspects of all three structures resides in their packing organization, mainly ruled by their hydrogen-bonding scheme. Non-covalent interactions for all three structures are presented in Table 3. The second column represents a code characterizing the interaction, for easy of reference: in what follows, any '#n' code will refer to a non-covalent interaction as listed in Table 3.

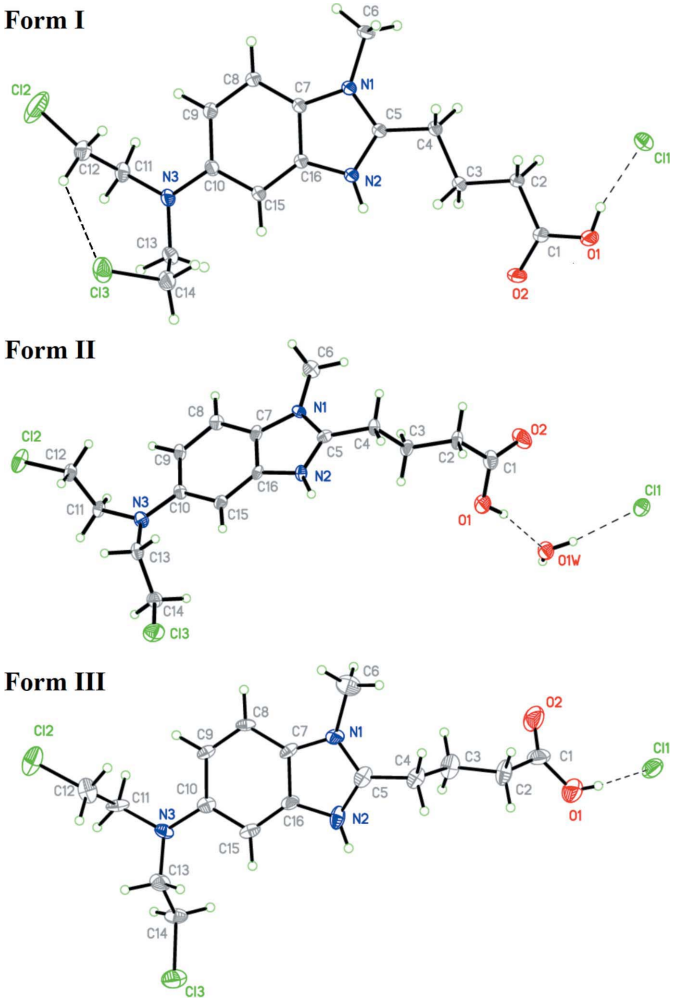

Figure 1
Molecular representations of forms (I), (II) and (III). Displacement ellipsoids drawn at a 40% level. Dashed lines indicate hydrogen bonds.

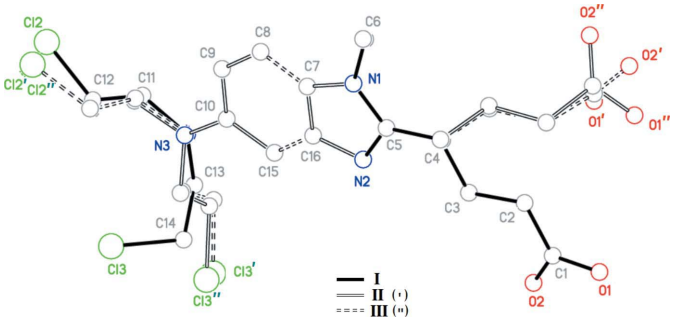

Figure 2
Superposition of forms (I), (II) and (III), through a least-squares fit of the aminobenzimidazole groups.

Table 2
Selected torsion angles (°) showing the largest differences.

	(I)	(II)	(III)
O1—C1—C2—C3	−175.5 (1)	52.6 (7)	127 (1)
O2—C1—C2—C3	5.2 (2)	−128.6 (6)	−48 (2)
C3—C4—C5—N1	−178.5 (1)	82.5 (7)	82 (2)
C3—C4—C5—N2	0.3 (2)	−92.9 (6)	−93.2 (2)
C13—N3—C10—C9	−179.5 (1)	161.3 (5)	158 (1)
C13—N3—C10—C15	0.5 (2)	−18.8 (7)	−23 (1)
C13—N3—C11—C12	103.4 (1)	−81.5 (6)	−80 (1)
C10—N3—C13—C14	74.7 (1)	94.6 (2)	98 (1)
N3—C11—C12—Cl2	166.92 (8)	−178.8 (4)	−179.3 (9)
N3—C13—C14—Cl3	66.6 (1)	−173.4 (4)	−175.4 (9)

In the case of form (I), the crystal structure can be described as built up in a constructive sequence, as follows.

(*a*) Hydrogen bonds #1 and #2 and their symmetry related $(1-x, 2-y, 1-z)$ ones, define a couple of R_8^2 loops linking two bendamustine moieties into a dimeric unit [Fig. 3(*a*)]. The centrosymmetric dimers are basically planar, and allocate in the crystal parallel to *a,* in a slanted, nearly (061) orientation [Fig. 3(*b*)].

(*b*) These dimers stack along the shortest axis, *b*, and link to each other by a number of interactions on which the Cl1 ions plays a central role. The most relevant link is provided by a sequence of (O1—H1O)···Cl1···(H4*B*—C4) bridges, made up by hydrogen bonds #3 and #4, defining columns along [010]. The C—H···π (#5) and a C—H···Cl (#7) interactions reinforce the stacking.

(*c*) These [010] columns, in turn, interact with neighbouring ones through the remaining hydrogen-bonds (#6 and #8 to #13) and a Cl···Cl interaction (#14). Fig. 4 shows a view of the crystal structure down the column axis, where one column has been highlighted, for clarity. The resulting 3D crystal structure is rather compact, as assessed by its larger-than-usual Packing Index (Kitaigorodskii, 1961), measuring the Percent Filled Space, and which calculated by *PLATON* (Spek, 2009) is 70.2. Expected values for organic structures lay in the range 66–68.

Incidentally, it is worth highlighting the charge withdrawal effect which the imidazole ring exerts on the methyl group at N1, and responsible of the hydrogen-bonding activation of its three (usually passive) hydrogens, all of which make structurally important, albeit weak, hydrogen-bonding interactions to the Cl1 ion (#7,#8,#9).

Given the structural relationship linking the hydrated structure (II) and its topotactically dehydrated form (III), in what follows we shall proceed in a comparative (rather than individual) analysis of the hydrogen-bonding schemes, and the 3D structure they give raise to.

Fig. 5(*a*) displays the centrosymmetric dimeric unit, the building block of the (II) structure. The encircled zone highlights the interaction region, showing the role which the water molecule plays as an intermediate link between Cl1 and the bendamustine moieties. In this particular link, the chlorine–

Table 3
Hydrogen-bond geometry and further non-covalent interactions (Å, °).

Form	Code	D—H···A	D—H	H···A	D···A	D—H···A
(I)						
	#1	N2—H2N···O2^{i}	0.85 (1)	1.89 (1)	2.7293 (13)	169 (2)
	#2	C15—H15···O1^{i}	0.95	2.42	3.3283 (14)	159
	#3	O1—H1O···Cl1	0.84 (2)	2.07 (2)	2.8994 (10)	170 (2)
	#4	C4—H4B···Cl1^{ii}	0.99	2.68	3.6325 (11)	161
	#5	C3—H3A···Cg2^{ii}	0.99	2.78	3.6325 (11)	161
	#6	C4—H4A···Cl1^{iii}	0.99	2.79	3.7105 (11)	156
	#7	C6—H6A···Cl1^{ii}	0.98	2.96	3.8640 (14)	154
	#8	C6—H6B···Cl1^{iii}	0.98	2.82	3.7314 (12)	156
	#9	C6—H6C···Cl1^{iv}	0.98	2.76	3.6510 (12)	152
	#10	C8—H8···Cl1^{iv}	0.95	2.93	3.7904 (11)	151
	#11	C13—H13B···Cl3^{v}	0.99	2.87	3.8502 (12)	169
	#12	C14—H14B···Cl3^{vi}	0.99	2.96	3.6600 (13)	128
	#13	C12—H12B···Cl3	0.99	2.79	3.5053 (14)	130
		Cl···Cl contact	d(Cl···Cl)			
	#14	Cl1···Cl3 ^{vii}	3.4840 (6)			
Symmetry codes for (I): (i) $-x+1, -y+2, -z+1$; (ii) $x, y-1, z$; (iii) $-x+\frac{1}{2}, -y+\frac{5}{2}, -z+1$; (iv) $-x+\frac{1}{2}, -y+\frac{3}{2}, -z+1$; (v) $-x+\frac{3}{2}, y-\frac{1}{2}, -z+\frac{3}{2}$; (vi) $-x+\frac{3}{2}, y+\frac{1}{2}, -z+\frac{3}{2}$; (vii) $x-\frac{1}{2}, -y+\frac{3}{2}, z-\frac{1}{2}$.						
(II)						
	#1	O1—H1O···O1W	0.84 (2)	1.82 (2)	2.657 (6)	171 (6)
	#2	N2—H2N···Cl1^{i}	0.85 (2)	2.20 (2)	3.048 (5)	176 (6)
	#3	C6—H6A···O2^{ii}	0.98	2.432	3.383 (7)	164
	#4	C6-H6B···Cl1^{ii}	0.98	2.841	3.646 (7)	139.9
	#5	C6—H6C···O2^{iii}	0.98	2.45	3.287 (7)	143
	#6	C8—H8···Cl1^{iii}	0.95	2.81	3.747 (6)	167
	#7	C12—H12A···Cl3^{iv}	0.99	2.98	3.882 (6)	152
	#8	C13—H13A···Cl2^{v}	0.99	2.88	3.690 (6)	139
	#9	C14—H14A···Cl1^{vi}	0.99	2.80	3.775 (6)	170
	#10	O1W—H1WA···Cl1	1.11 (5)	2.01 (5)	3.114 (4)	172 (5)
	#11	O1W—H1WB···Cl1^{vii}	0.85 (1)	2.49 (3)	3.264 (4)	151 (5)
	#12	C11—H11B Cg2^{vii}	0.99	2.87	3.656 (6)	137
		π···π contact	d(π···π)	Dihedral angle		
	#13	Cg2···Cg1 ^{vii}	3.553 (3)	0.6 (3)°		
		Cl···Cl contact	d(Cl···Cl)			
	#14	Cl2···Cl3 ^{viii}	3.575 (2)			
Symmetry codes for (II): (i) $-x+1, -y, -z$; (ii) $-x+1, -y, -z+1$; (iii) $-x+2, -y, -z+1$; (iv) $x, y, z+1$; (v) $x, -y+\frac{1}{2}, z-\frac{1}{2}$; (vi) $-x+2, -y, -z$; (vii) $x+1, y, z$, (viii) $x+1, y, z+1$.						
(III)						
	#1	O1—H1O···Cl1	0.85 (2)	2.29 (9)	3.036 (10)	147 (15)
	#2	N2—H2N···Cl1^{i}	0.85 (2)	2.18 (3)	3.024 (12)	171 (14)
	#3	C6—H6A···O2^{ii}	0.98	2.49	3.438 (18)	163
	#4	C6—H6B···Cl1^{ii}	0.98	3.026	3.651 (19)	124
	#5	C6—H6C···O2^{iii}	0.98	2.41	3.329 (18)	156
	#6	C8—H8···Cl1^{iii}	0.95	2.78	3.696 (12)	162
	#7	C12—H12A···Cl3^{iv}	0.99	2.91	3.838 (16)	156
	#8	C13—H13A···Cl2^{v}	0.99	2.95	3.743 (14)	138
	#9	C14—H14A···Cl1^{vi}	0.99	2.84	3.824 (15)	172
	#10	C11—H11B···Cg2^{vii}	0.99	2.83	3.612 (5)	135
		π···π contact	d(π···π)	Dihedral angle		
	#11	Cg2···Cg1 ^{vii}	3.581 (3)	1.0 (7)°		
		Cl···Cl contact	d(Cl···Cl)			
	#12	Cl2···Cl3 ^{viii}	3.544 (4)			
Symmetry codes for (III): (i) $-x+1, -y, -z$; (ii) $-x+1, -y, -z+1$; (iii) $-x+2, -y, -z+1$; (iv) $x, y, z+1$; (v) $x, -y+\frac{1}{2}, z-\frac{1}{2}$; (vi) $-x+2, -y, -z$; (vii) $x+1, y, z$; (viii) $x+1, y, z+1$.						

water interaction is so strong that the $(O—H)_{water}$ distance enlarges significantly (see refinement section). On dehydration, the dimeric unit is kept, but water removal has the effect of forcing a Cl1 movement towards O1, as well as slight rotation of the carboxylato end, to facilitate the (substituting) Cl1···H1O interaction. The process gives raise to perceivable shrinkage (∼3%) along the unique axis [$b_{(II)}$ = 47.213 (5) Å, $b_{(III)}$: 45.671 (19) Å].

Fig. 6, in turn, shows the way in which the planar dimers stack along the short *a* axis, to form [100] columns. In structure (II) [Fig. 6(*a*)] the remaining water hydrogen makes a strong bond (#11) along the columnar direction, complemented by weaker C—H···π (#12) and π···π (#14) interactions. In the process, a strong ···(HOH)···Cl···(HOH)··· backbone builds up (highlighted). It is perhaps this particular hydration water distribution, much in the way as the *channel hydrates* filling one-dimensional channels (Falk & Knop, 1973) which allows for an easy input–output of water molecules in the structure (see below). After water removal, the dimeric stacking remains, but the linkage is much weaker [Fig. 6(*b*)].

The final result is shown in Fig. 7, with columns interacting laterally through second-order interactions (codes as given in

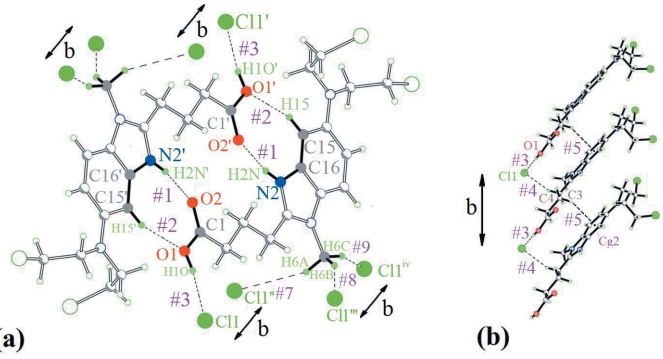

Figure 3
(*a*) The dimeric unit in (I). (*b*) Stacking of dimeric units in (I).

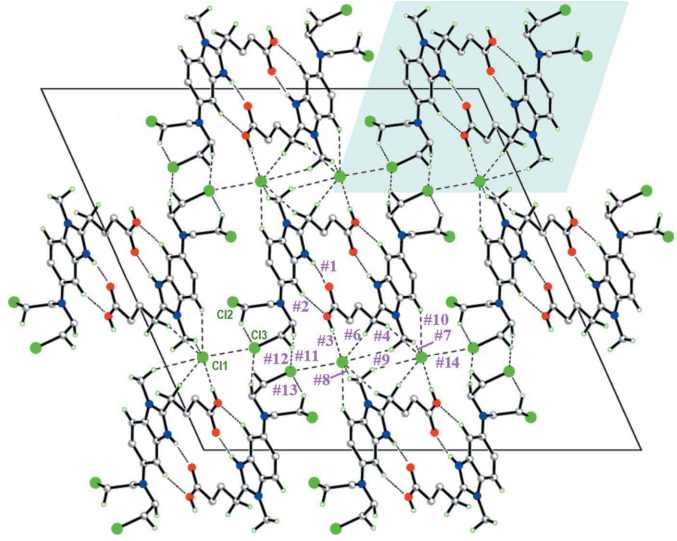

Figure 4
A packing view of (I) along **b**. Highlighted, a dimeric unit in projection.

Table 3). Highlighted in Fig. 7(*a*), one of the dimeric units, seen in projection.

The Packing Indexes values [69.3 and 67.7 for (II) and (III), respectively], could be considered a final summary of the differences in packing interactions, showing the hydrated structure to be much better packed than the dehydrated one. In spite of this there are no perceivable voids in the latter structure.

At this stage is possible to correlate some structural differences in the molecular conformation of (I) and (II), (III), in particular the ones referring to the tails. At the carboxylato end, with the carboxylato group in (I) entering in direct link to a neighbouring bendamustine moiety through closed R_8^2 loops (#1, #2) while interacting with O1*W* in (II) (#1) or Cl1 in (III) (#1).

Regarding the nitrogen mustard tails, both in forms (II) and (III) the terminal Cl2 and Cl3 atoms adopt *anti*-conformation to N3 [N3—C11—C12—Cl2 = −178.8 (4)° and 179.3 (9)°, N3—C13—C14—Cl3 = −173.4 (4)° and −175.4 (9)° for (II) and (III), respectively], with what both branches are wide apart, far from any possible intramolecular C—H···Cl interaction. In form (I), instead, both branches present different conformations, the one involving Cl2 is *anti* [N3—C11—C12—Cl2 = 166.92 (8)°] while the one involving Cl3 is *gauche* [N3—C13—C14—Cl3 = 66.6 (1)°]. This particular configuration allows Cl3 to approach the Cl2 branch, thus facilitating the existence of an intramolecular C—H···Cl bond linking tails (#13). The difference in molecular geometries can be easily assessed by the Cl···Cl distance in each form {d[Cl2$_{(I)}$···Cl3$_{(I)}$] = 5.09 Å, d[Cl2$_{(II)}$···Cl3$_{(II)}$] = 7.17 Å, d[Cl2$_{(III)}$···Cl3$_{(III)}$] = 7.04 Å}.

Trying to found out some statistics on the appearance of nitrogen mustard tails in the literature we made a search in the CSD of molecules presenting the same C—N(CH$_2$—CH$_2$Cl)$_2$ group. We found 38 hits in 35 structures, 13 of which showed to be *anti–anti*, five *gauche–gauche* and the remaining 21 presented an *anti–gauche* conformation. Among them, only eight presented some kind of intra-branch interaction in the form of C—H···Cl contacts, as in (I).

There are no obvious structural similarities between the anhydrated forms (I) and (III); something expectable, given the way in which form (III) was obtained.

According to the Density Rule (Burger & Ramberger, 1979) which states that the structure with the higher density should be the more stable one, form (I) (with a density of 1.445 g cm^{-3} and a packing index of 70.2) is more stable than form (III) (which has a density of 1.395 g cm^{-3}, and a packing index of 67.7). Even if this stability relation is valid at −123°C,

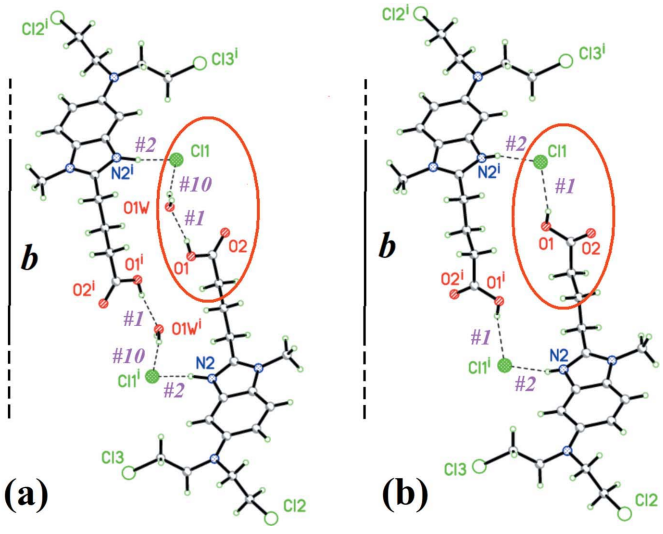

Figure 5
The dimeric unit in (II) (*a*) and (III) (*b*). The water molecule role is highlighted in the red circle.

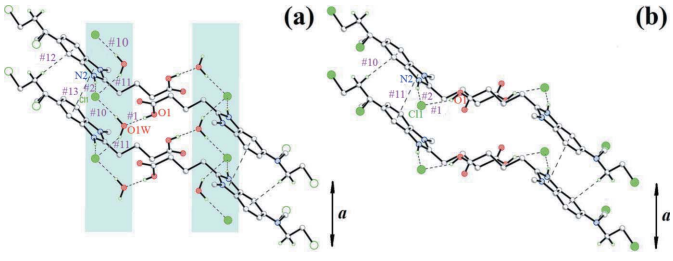

Figure 6
Staking of dimers in (II) (*a*) and (III) (*b*). Highlighted, the ···(HOH)···Cl···(HOH)··· *backbone* chain, encircled in Fig. 5(*a*).

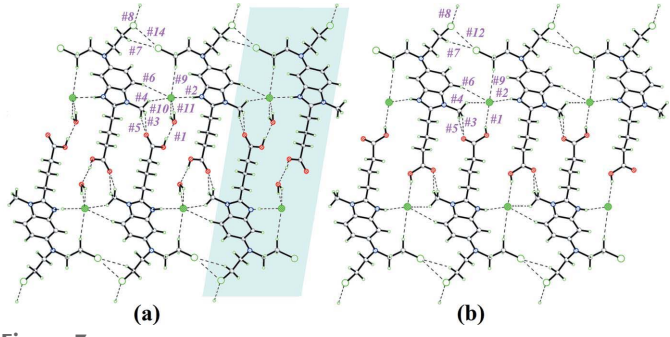

Figure 7
Packing view of (II) (*a*) and (III) (*b*) along the column direction [100]. Highlighted, a dimeric unit in (II).

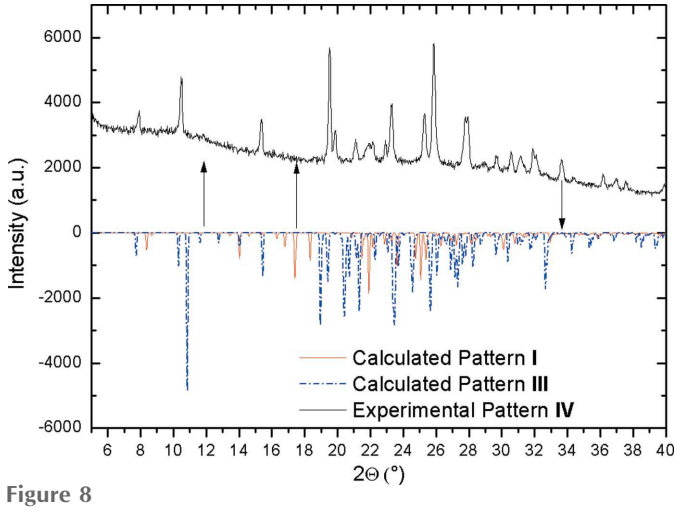

Figure 8
XRPD diffraction pattern measured of form (IV). On the negative *y* axis calculated patterns of forms (I) and (III) are shown.

(temperature at which structural measurements were performed), the DSC experiments show that this relation holds for the whole temperature range below the melting point of form (III).

Since the structural differences between forms (II) and (III) are small, it is reasonable to suppose that the internal energies between both structures will differ less than those between (II) and (I), where the structural differences are larger. Thus, the (II)→(III) transformation would follow Ostwald's step Rule (Ostwald, 1897) which states that upon dehydration form (II) should transform into the structure with the closest energy.

Despite the fact that no single crystals could be obtained for form (IV), its XRPD pattern was collected in order to determine if this was a different form than those previously described. Fig. 8 shows, on the positive side of intensities, the measured XRPD pattern for form (IV) (the rather high background is indicative of the presence of amorphous material in the sample). Furthermore, in the negative side of intensities the calculated patterns for forms (I) and (III) are shown, for comparison. Differences are apparent (the most conspicuous marked with an arrow) with what form (IV) can actually be considered a different form.

3.2. TG and DSC measurements

Thermogravimetric (TGA) and differential scanning calorimetry (DSC) measurements were performed for forms (I), (II) and (IV), with a heating rate of 10°C min^{-1}.

TGA. Form (II) shows a total mass loss of 4.3%, starting at approximately 45°C. This corresponds to a whole molecule of water per molecule of bendamustine (theoretical: 4.36%), compatible with the transformation from (II) to (III) seen in SCXRD measurements after thermal dehydration. After this event, (II) does not present any further mass loss below 200°C. Fig. 9 shows the mass curves as a function of the temperature for these measurements.

Forms (I) and (IV), in turn, do not show significant mass losses below 200°C.

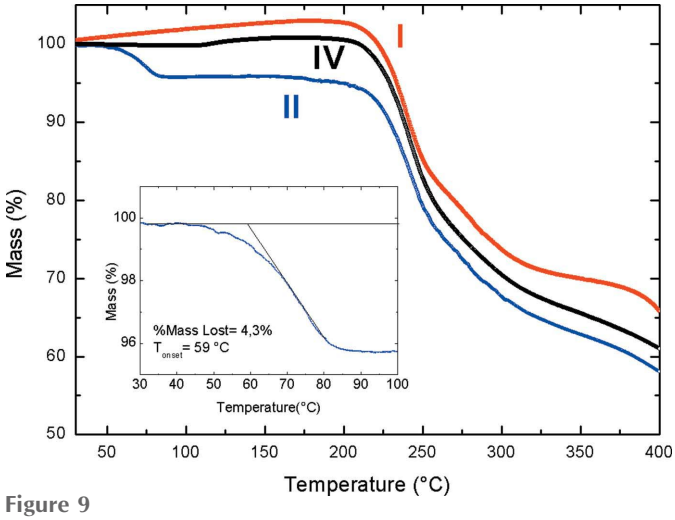

Figure 9
Thermogravimetric (TG) measurements for (I), (II) and (IV).

DSC. Fig. 10 shows the DSC diagrams of (I), (II) and (IV). Inspection of the figure assesses that (I) presents the higher melting point. On the other side, its heat of fusion is higher than the one for form (III), and according to the rules stated in Burger & Ramberger (1979), this is indicative of a monotropic system. (The heat of fusion rule states that if the higher melting polymorph has the lower enthalpy of fusion, then the two forms are enantiomerically related.) If, as in this case, the higher melting polymorph has the higher enthalpy of fusion, then the two forms are monotropically related and the higher melting polymorph [form (I)] is the most stable one.

Form (IV) shows a broader peak, indicative of the presence of impurities in the sample (Giron & Goldbronn, 1995). It is possible, due to the obtainment method used that the sample may include amorphous bendamustine hydrochloride. Therefore, the resulting value for the enthalpy change of form (IV) is probably lower than the actual one for an eventual pure sample. Despite this, the fusion peak should not be very different from the one for an uncontaminated sample. After fusion, all samples were cooled at 10°C min^{-1} up to 20°C, and in all cases the resultant amorphous shows the same glass transition at approximately 50°C, suggesting that the three forms transform into the same amorphous form. It can thus be concluded that form (IV) has not suffered any chemical reaction in its generation process and is actually another polymorphic form of bendamustine hydrochloride. The corresponding DSC curves for the cooling of the molten bendamustine hydrochloride are shown in Fig. S1 in the supporting information.

Summarizing: by observing the fusion peaks [(I): 168°C; (III): 155°C, (IV): 163°C] and their enthalpy of fusion, we can establish that the most stable form is (I), and the least stable one is (III).

Even though the results are not conclusive, it appears that the relationship between (III) and (IV) is monotropic according to the heat of fusion rule [the one for (IV),

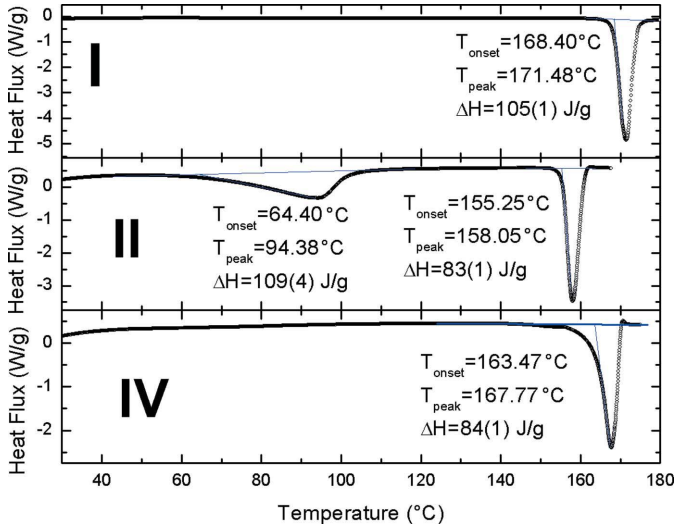

Figure 10
DSC pattern for (I), (II) and (IV). After dehydration at T_{onset} = 64.4°C, (II) transforms into (III).

$\sim$84 J g^{-1} is higher than the one for (III)]. Eventual impurities in the sample of (IV) could no invalidate the arguments, since the heat of fusion of the pure sample would not be smaller.

On the other hand, the relationship between forms (I) and (IV) is also monotropic: the heat of fusion obtained for form (IV) ($\sim$84 J g^{-1}) is significantly smaller than the one for form (I), ($\sim$105 J g^{-1}). Since the eventual presence of impurities in the sample of form (IV) would not explain that difference, it is reasonable to infer a monotropic relationship between them.

3.3. Stability under high-humidity conditions

Form (I): mass measurements of form (I) shows a sudden change in water adsorption after one day of exposure to a high-humidity environment. This fact could be attributed to the crystalline structure collapse of form (I) in these conditions. After this, the sample adsorbs water until duplication of its own weigh. Fig. 11 shows the XRPD pattern obtained after different times at high-humidity conditions and the mass curve for the sample as a function of time. After one day, form (I) transforms almost entirely into amorphous material, with only a few recognizable Bragg peaks, much weaker than those in the starting material. The amorphization process is completed in 48 h, after which no Bragg peaks can be observed in the diffractogram. Incidentally, this amorphous form is optically different from the one obtained by supercooling of the molten bendamustine hydrochloride (Fig. S2 in supporting information).

After 231 days of storage at high-humidity conditions, it was found that the amorphous material so obtained was fully converted into form (II): this form did not show any changes in its XRPD, probably indicating that this is the highest possible hydration state attainable for bendamustine hydrochloride, with the sample not suffering any change of state in these high-humidity conditions. In spite of this, there is some mass gain, probably due to hygroscopicity.

Form (III): during a 24 h treatment, the XRPD diagram shows slight modifications, [consistent with a transformation into (II)] and remaining stable afterwards. Mass measurement, in turn, shows a change also compatible with the transformation from (III) to (II). From these data it appears that 24 h can be safely considered an upper bound for the time needed to transform form (III) into form (II) under these high-humidity conditions.

3.4. Stability of (II) under low-humidity conditions

Fig. 12 shows the mass changes that occurred during the experiment. In less than 30 minutes about 1% of the sample mass was lost. This corresponds to approximately one-quarter water molecule per bendamustine unit. Despite this being less than the amount of water in the structure, it is possible that the sample is in form (III) and the rest of the water molecules are adsorbed by the sample in a disordered form. XRPD measurements do not help to clarify this fact because of the small differences between XRPD patterns of forms (II) and (III). Nevertheless some small changes can be observed in the intensities of the Bragg peaks, compatible with a transformation into (III) (Fig. 12). Even though it is difficult to establish quantitatively changes in the sample, it appears they take place within a few hours.

4. Conclusions

The crystal structures of three different forms of bendamustine hydrochloride [(I), (III): anhydrous, (II): monohydrate] are discussed. Difference in molecular conformation, mainly in the terminal tails, should be attributable to packing. Form (II) behaves as a channel hydrate and can be topotactically dehydrated into form (III). A fourth form, (IV), was obtained, though only in powder from.

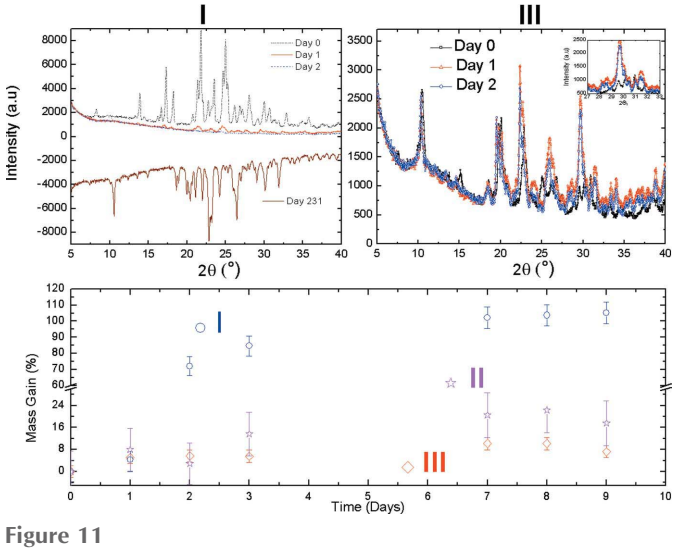

Figure 11
Above: X-ray powder diffraction patterns for (I) and (III), after exposure to a high-humidity environment. [The 231 days storage case of (I), drawn with inverted intensities, for clarity.] Below: Mass gain measurements as a function of time, for (I), (II) and (III).

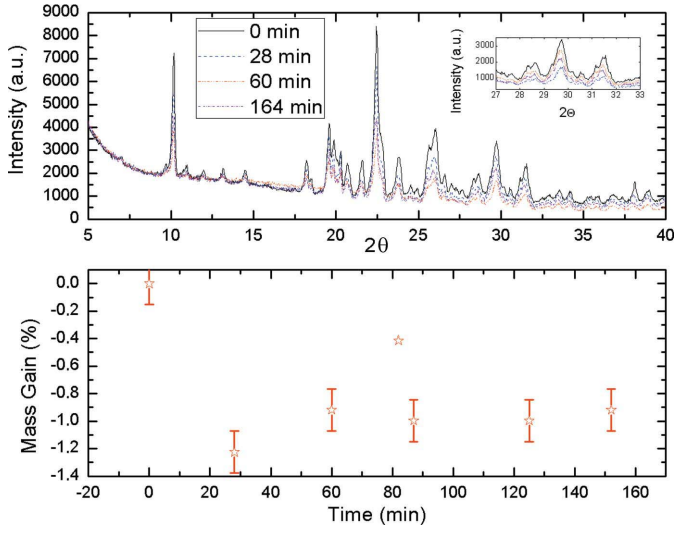

Figure 12
Diffraction pattern and mass gain as a function of time for (II), while kept in a dry environment.

Thermal studies were performed, disclosing a monotropic relationship between (I), (III) and (IV). The relative stability between the different forms has also been established, the most and less stable forms being (I) and (III), respectively.

Forms (I) and (III) were studied under high-humidity conditions, where they proved to be unstable. Form (II), in turn, was studied under low humidity, showing it can easily transform into form (III) in less than 24 h.

These results suggest that special care should be taken in storage of these forms of bendamustine hydrochloride [(I), (II), (III)] due to their instability under different humidity conditions. These characteristics may have impact on parenteral formulations using any of these forms. The stability results obtained for form (IV) are inconclusive, and further studies should be performed. For this to be possible, however, an alternative method of production should be found, so as to make sure that no amorphous material is present in the sample.

Acknowledgements

We acknowledge Laboratorios Eriochem for kindly providing bendamustine hydrochloride in its hydrate form.

References

Akers, M. J. (2002). *J. Pharm. Sci.* **91**, 2283–2300.
Bremer, K. & Roth, W. (1996). *Diagn. Ther.* **17**, 1–6.
Burger, A. & Ramberger, R. (1979). *Mikrochim. Acta*, **72**, 259–271.
Cheson, B. & Rummel, M. (2009). *J. Clin. Oncol.* **27**, 1492–1501.
Cooper, M. I., Courvoisier, L. D., Eddleston, M. & McKean, E. (2009). United States Patent Application Pub. No.: US 2009/0264488 A1.
Drager, A. S., Labell, R. Y. & Patel, P. R. (2012). United States Patent Application 20120129904.
Falk, M. & Knop, O. (1973). *Water. A Comprehensive Treatise*, Vol. 2, edited by F. Franks, pp. 55–113. New York: Plenum Press.
Giron, D. & Goldbronn, C. (1995). *J. Therm. Anal.* **44**, 217–251.
Groom, C. R., Bruno, I. J., Lightfoot, M. P. & Ward, S. C. (2016). *Acta Cryst.* B**72**, 171–179.
Kitaigorodskii, A. I. (1961). *Organic Chemical Crystallography*. New York: Consultants Bureau.
Ostwald, W. (1897). *Z. Phys. Chem.* **22**, 289–330.
Ravikanth, M., Babu, P. S., Rao, M. V. B. & Allamneni, Y. (2013). *Int. J. Pharm. Sci. Rev. Res.* **23**, 89–93.
Reck, G. (2006). CSD Private communication, entry NEQGUM.
Rigaku Oxford Diffraction (2015). *CrysAlis PRO*. Rigaku Oxford Diffraction, Yarnton, England.
Sheldrick, G. M. (2008). *Acta Cryst.* A**64**, 112–122.
Sheldrick, G. M. (2015). *Acta Cryst.* A**71**, 3–8.
Spek, A. L. (2009). *Acta Cryst.* D**65**, 148–155.
Yu, L., Milton, N., Groleau, E. G., Mishra, D. S. & Vansickle, R. E. (1999). *J. Pharm. Sci.* **88**, 196–198.